Korean J. Chem. Eng., 38(1), 46-54 (2021)
DOI: 10.1007/s11814-020-0684-1

pISSN: 0256-1115
eISSN: 1975-7220

Facile fabrication of copper oxide modified activated carbon composite for efficient CO_2 adsorption

Guanghui Chen*, Fei Wang*, Shougui Wang, Cailin Ji*, Weiwen Wang*, Jipeng Dong*, and Fei Gao*,†**

*Shandong Key Laboratory of Reactions and Isolations of Muti-phase Liquid, College of Chemical Engineering, Qingdao University of Science & Technology, Qingdao, 266042, China
**Fundamental Chemistry Experiment Center (Gaomi), Qingdao University of Science & Technology, Gaomi, 261500, China
(*Received 10 June 2020 • Revised 6 September 2020 • Accepted 21 September 2020*)

Abstract−Copper oxide modified activated carbon (CuO/AC) composites for the CO_2 capture were synthesized *via* a facile assembly strategy associated with a direct solid-state heat dispersion process by introducing CuO into AC using $Cu(NO_3)_2$ as the copper source. The synthesized CuO/AC composites with various CuO contents were characterized by powder X-ray diffraction, scanning electron microscopy and nitrogen adsorption-desorption measurement, and the CO_2 adsorption performance was investigated. The characterization results indicate that the $Cu(NO_3)_2$ species was well dispersed into the AC pore channels and then converted to a highly dispersed CuO after the activation process. The adsorption results reveal that the CO_2 adsorption performance can be significantly improved by introducing CuO onto the AC surfaces, and the CuO(0.6)/AC composite with a CuO loading of 0.6 mmol/g AC shows a high CO_2 adsorption capacity and adsorption selectivity and displays an excellent reversibility. Additionally, the calculated adsorption heat values of CO_2 on the CuO(0.6)/AC composite are in the range of 27.3 to 33.9 kJ/mol.

Keywords: CuO/AC Composite, CO_2, Adsorption, Solid-state Heat Dispersion, Selectivity

INTRODUCTION

CO_2 is a major greenhouse gas that contributes more than two-thirds of the global warming effect [1]. Excessive anthropogenic CO_2 emissions, mainly released from the coal-fired power plant flue gases, have already affected the climate change and caused some serious consequences, including the continued global sea level rise and more frequent extreme weather events [2]. Although renewable energy technologies have attracted more and more attention in recent years to alleviate energy shortage and greenhouse gas emissions, the traditional energy sources, including coal, oil and natural gas, will continue to be the primary sources for the increasing global energy demand in the near future [3]. Consequently, growing efforts have been focused on developing the efficient CO_2 capture technologies [4-6]. Currently, the liquid amine absorption under atmospheric pressure is the most well-known mature technology for the CO_2 separation from flue gases, but have some disadvantages, such as the high energy requirement for the regeneration process, the high equipment corrosion, the high vapor pressure, and the easy degradation of solvent [7,8].

Adsorption technology is a promising alternative for capturing CO_2 from flue gases due to its low operation costs, easy operation and low energy consumption [9]. Nonetheless, to successfully use the adsorption technology for CO_2 capture applications, there are three main aspects needed to be addressed: the selection of adsorbent, the regeneration strategy, and the reactor configuration. A number of porous materials [10-12], including metal-organic frameworks (MOFs), molecular sieves, alumina powders, and carbon materials, are widely used for the gas adsorption and storage. Among them, activated carbon (AC) is a versatile porous material due to its high porosity, high specific surface area, excellent adsorption property, easy-to-design structure, high surface reactivity, adequate mechanical strength, low cost as well as abundant reserves. It has been widely used in the catalysis and adsorption separation fields [13,14]. The excellent structural properties make activated carbons exhibit a good CO_2 capture performance, but the adsorption is commonly caused by the physical interaction, resulting in that the adsorbent is sensitive to the temperature and the adsorption selectivity is relatively poor. Thus, many studies have focused on the chemical modification for AC surfaces aiming to improve the capture capacity and adsorption selectivity for CO_2.

According to the CO_2 mildly acidic nature, the modification of the activated carbon surfaces by introducing basic functional groups (such as amine groups and metal oxides) can improve the CO_2 capture performance [15-17]. Amine-functionalized AC composites achieve a high CO_2 adsorption performance; however, their stability needs to be further enhanced [18,19]. And the CO_2 capture performance can be significantly improved by introducing alkali metal and alkali earth metal species into the porous material structures [20-23]; however, these materials need a high regeneration temperature to decompose metal carbonate to metal oxide. Recently, transition metal-based adsorbents have attracted great attention for the CO_2 capture [24-28]. Transition metal oxides can bond CO_2 molecules through π-complexation interactions by forming both the σ bond and the back donation π bond. This interaction is stronger than the physisorption, so transition metal based adsor-

†To whom correspondence should be addressed.
E-mail: feigao@tju.edu.cn

bents can achieve a higher adsorption capacity and adsorption selectivity for CO_2. In addition, for an adsorbent in the practical adsorption process, beside the high adsorption capacity and adsorption selectivity, a reliable and economical adsorbent regeneration strategy is also very important for realizing the multiple adsorption and desorption cycles. Currently, an industrial adsorbent can be regenerated by the pressure swing or temperature swing adsorption (PSA and TSA) operations based on the periodic variation of the pressure or temperature of the adsorption unit [29]. Among them, TSA processes are considered to be more appropriate for the post-combustion CO_2 capture since it can avoid the compression and/or application of vacuum to the large amount of gaseous stream required in PSA processes, significantly reducing the energy consumption [30,31]. In particular, for the chemical adsorbent regeneration, TSA process is preferred to PSA process since a simple variation of the pressure is not efficient enough to achieve a complete regeneration of the adsorbent due to the strong chemical interactions of the adsorbents with CO_2 [32]. For the transition metal-based adsorbents, the interaction of CO_2 with the adsorbent *via* π-complexation is between physisorption and chemisorption, and the adsorbents can be easily regenerated by utilizing a TSA operation [33,34].

Generally, the loading of transition metal oxides onto the porous materials surfaces is mainly prepared by the electroplating or wet-impregnation methods, which are intensive preparation processes. In addition, the dispersion degree of transition metal oxides on support surfaces obtained through a traditional impregnation method is closely related to numerous parameters [35], and the added transition metal precursor cannot be completely impregnated into the support channels for the impregnation method, thus leading to a metallic species waste. Solid-state grinding method is a facile and efficient approach for introducing metal components into the pore channels of the porous supports [36,37]. This method can completely introduce the metal precursor into the support and can yield a highly dispersed metal species on the surfaces of the supports.

Herein, transition metal copper oxide (CuO) was introduced into the porous AC by a solid-state grinding approach without using any solutions. The main aim of this work is to synthesize CuO/AC composites by a facile approach for the efficient CO_2 adsorption. The synthesized CuO/AC composites with various CuO loadings were characterized by powder X-ray diffraction (XRD), scanning electron microscopy (SEM) and nitrogen adsorption-desorption measurement to investigate their structural properties, and the CO_2 adsorption performance was investigated including the CO_2 adsorption capacity, the CO_2/N_2 adsorption selectivity, the cyclic stability and the adsorption heat.

EXPERIMENTAL

1. Materials

Activated carbon was obtained from Chengde Xingyuan Activated Carbon Co., Ltd., $Cu(NO_3)_2{\cdot}3H_2O$ (AR) was obtained from Tianjin Guangfu Fine Chemical Research Institute, and NH_4NO_3 (AR) was obtained from Tianjin Kemiou Chemical Reagent Co., Ltd. All the gases were supplied by Qingdao Dehai Gas Co., Ltd. with a purity of more than 99.9%.

2. CuO/AC Composites Preparation

The CuO/AC composites were prepared as follows: the calculated amounts of activated carbon and $Cu(NO_3)_2{\cdot}3H_2O$ powder was thoroughly mixed by grinding, and then the resulting powder was activated at 423 K for 4 h in air, and 623 K for 4 h under the N_2 flowing. The composites with various copper content of 0.2, 0.4, 0.6, 0.8 and 1.0 mmol/g AC support were synthesized. Before and after the activation, the samples are named as $Cu(NO_3)_2$(X)/AC and CuO(X)/AC, respectively, where X is the copper loading per gram activated carbon in mmol.

3. Composites Characterization

The XRD patterns were collected using a D/max-2500 (Rigaku, Japan) diffractometer with Cu Kα radiation (λ=1.5406 Å) from 10° to 80°. The textural properties of the prepared adsorbents were determined by the nitrogen physisorption performed on a TriStar 3000 system (Micromeritics, USA) at 77 K after degassing under vacuum at 473 K for 4 h. The SEM images were performed by a Sigma-500 (ZEISS, Germany) instrument to analyze the composite morphology.

4. Adsorption Measurements

CO_2 and N_2 adsorption measurements were performed by a Quantachrome Autosorb-iQ instrument with a pressure range of 0-101.3 kPa at the setting temperature controlled by a circulation bath. Before each adsorption measurement, the adsorbents were treated under vacuum at 473 K for 4 h.

5. Theory and Method

5-1. Adsorption Isotherm Fitting

Numerous adsorption isotherm equations, such as Freundlich [38], Langmuir [39], Sips [40], and Toth [41] have been developed to describe the adsorption isotherms. In this work, the adsorption data of CO_2 and N_2 on the adsorbents were correlated using the Sips equation as expressed by:

$$q = q_m \frac{bp^{1/n}}{1+bp^{1/n}} \tag{1}$$

where q and q_m are the adsorption amount at the equilibrium pressure p (kPa) and the maximum adsorption amount (mmol/g), respectively, b is the affinity coefficient (kPa^{-1}), and n is a dimensionless parameter.

5-2. Calculation of IAST Adsorption Selectivity

The ideal adsorbed solution theory (IAST), which is developed by Myers and Prausnitz [42], is a common and effective theoretical model for calculating the adsorption selectivity from pure component isotherms. In this work, IAST was used to calculate the CO_2/N_2 adsorption selectivity (S_{CO_2/N_2}), and commonly given by [43]:

$$S_{CO_2/N_2} = \frac{x_{CO_2}/x_{N_2}}{y_{CO_2}/y_{N_2}} \tag{2}$$

where x_{CO_2} and y_{CO_2} are the CO_2 mole proportions in the adsorbed phase and gas phase at equilibrium, respectively, and x_{N2} and y_{N2} are the N_2 mole proportions in the adsorbed phase and gas phase at equilibrium, respectively.

5-3. Isosteric Heat of Adsorption

The CO_2 adsorption isosteric heat on the CuO/AC composite at a specific CO_2 loading was determined by the Clausius-Clapeyron equation from the adsorption data at different temperatures [44]:

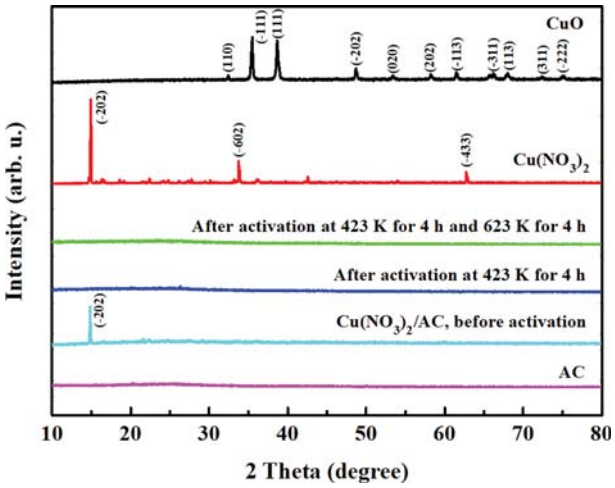

Fig. 1. XRD patterns of CuO, $Cu(NO_3)_2$, AC and $Cu(NO_3)_2$ loaded samples with the copper loading of 0.6 mmol/g AC before and after activation.

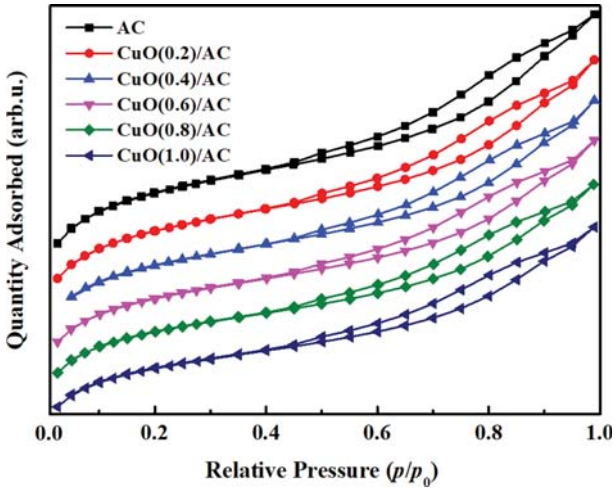

Fig. 2. Nitrogen adsorption and desorption isotherms at 77 K on AC support and CuO/AC composites with different CuO loadings.

$$Q_{st} = RT^2\left(\frac{\partial \ln p}{\partial T}\right)_{q_a} \quad (3)$$

where Q_{st} is the adsorption isosteric heat (kJ/mol), T is the adsorption temperature (K), q_a is a given CO_2 adsorption amount (mmol/g), and R is the universal gas constant (J mol^{-1} K^{-1}).

RESULTS AND DISCUSSION

1. Material Characterization

Fig. 1 presents the powder XRD patterns of pure CuO and $Cu(NO_3)_2$, the activated carbon support, and the supported $Cu(NO_3)_2$ composites with a copper loading of 0.6 mmol/g AC before and after the activation process. Before the activation, the $Cu(NO_3)_2$/AC sample shows the diffraction peak at 2θ value of 14.84° assigned to (-202) plane of $Cu(NO_3)_2$ which corresponds to JCPDS card No. 75-1493. After the activation at 423 K, the diffraction peaks of $Cu(NO_3)_2$ disappear. The behavior reveals that the $Cu(NO_3)_2$ species was well-dispersed into the AC support surfaces, and the absence of $Cu(NO_3)_2$ diffraction peaks in XRD pattern may be because the highly dispersed $Cu(NO_3)_2$ species in $Cu(NO_3)_2$/AC composite is too tiny to be observed by XRD. After the further activation at a higher temperature of 623 K for the decomposition of $Cu(NO_3)_2$ to CuO, no diffraction peaks attributed to CuO are observed in the sample, indicating that the CuO species might be present in a highly dispersed state on the surface of AC support. The high surface area of the AC support is conducive to the fine dispersion of the active species at low loading. In addition, there is another possibility that the CuO content in the CuO/AC sample with a copper loading of 0.6 mmol/g AC is too small to be detected by XRD, which is calculated to be about 4.6%. This possibility can be ruled out by an obvious observation of CuO diffraction peaks in the CuO/AC samples with lower CuO contents of 0.8% and 2% obtained with a traditional impregnation method by Yin et al. [45]. The results imply that the CuO/AC composite with highly dispersed CuO has been successfully synthesized using $Cu(NO_3)_2$ as copper sources by this approach.

Table 1. Textural properties of AC and CuO/AC composites

Samples	Total pore volume (cm^3/g)	BET surface area (m^2/g)
AC	1.30	1,450
CuO(0.2)/AC	1.20	1,383
CuO(0.4)/AC	1.19	1,319
CuO(0.6)/AC	1.15	1,277
CuO(0.8)/AC	1.08	1,213
CuO(1.0)/AC	1.03	1,156

Fig. 2 presents the nitrogen adsorption isotherms at 77 K of the AC support and the obtained CuO/AC composites with various CuO content. From Fig. 2, the nitrogen adsorption amount of the composites decreases gradually with an increase in the CuO loading. Table 1 shows a summary of the textural properties of the AC support and the CuO/AC composites. As shown in Table 1, the parent AC support displays a high total pore volume of 1.30 cm^3/g and specific surface area of 1,450 m^2/g, and the introduction of CuO in AC results in a reduction in the total pore volume and specific surface area compared to the parent AC sample. This phenomenon is attributed to the fact that the partial pore channels of the AC support are occupied by the introduced CuO species.

Fig. 3 presents the SEM images of the CuO(0.6)/AC and AC samples. In SEM images of the AC support (Fig. 3(a) and (b)), some irregularly shaped AC particles of different sizes are observed. These AC particles have a large number of pores, leading to a large pore volume and high specific surface area, which is beneficial to the CuO introduction. From the SEM images of CuO(0.6)/AC composite (Fig. 3(c) and (d)), it can be seen that there is no significant change in the primary structure after the CuO modification, and there is no obvious CuO aggregation on the CuO(0.6)/AC composite surfaces. This phenomenon reveals that CuO species was well dispersed into the AC support pore channels, which is also confirmed by the results of XRD. Additionally, compared with the par-

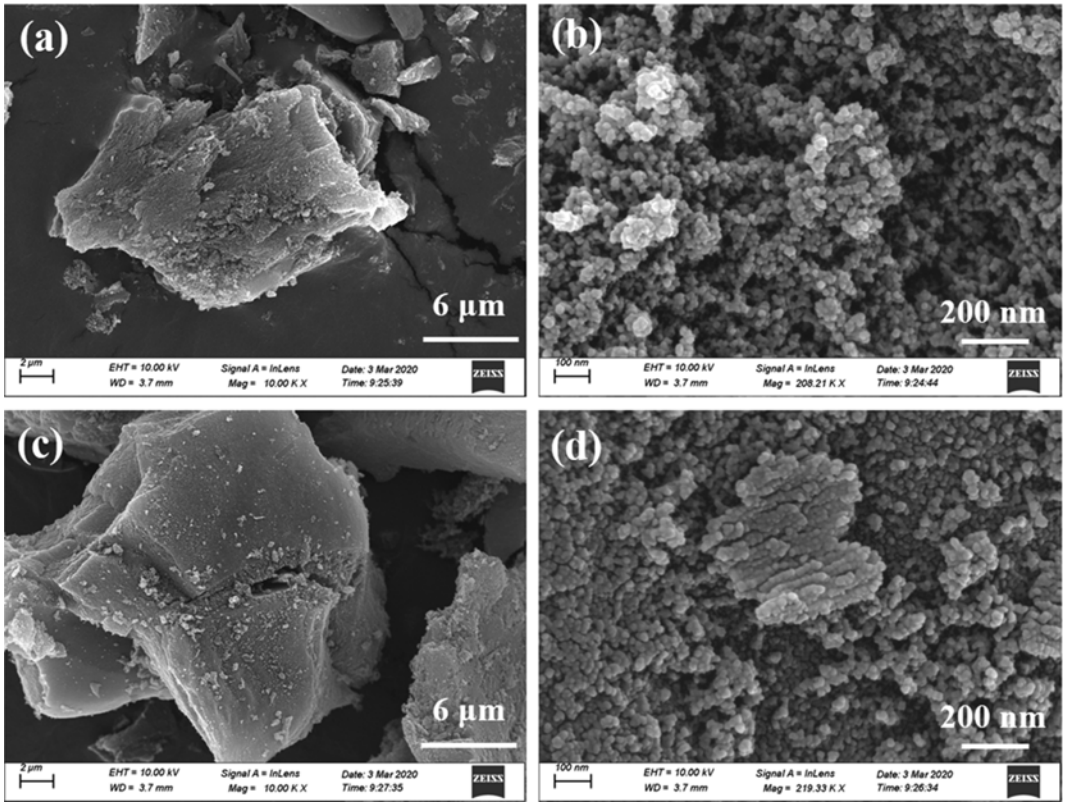

Fig. 3. SEM images of AC support ((a), (b)) and CuO(0.6)/AC composite ((c), (d)).

ent AC support, fewer internal pores are observed in the CuO(0.6)/AC composite, resulting from the occupation and blockage of partial AC support pores channels by CuO species, which is responsible for the reduction in the pore volumes and specific surface areas of the N_2 adsorption measurement results.

2. Adsorption Performance of CO_2 on CuO/AC Composites

The influence of the CuO content on the CO_2 adsorption amount of the CuO/AC composites is depicted in Fig. 4. It can be seen that the CO_2 adsorption capacity of all the CuO/AC composites is obviously higher than that of the parent AC sample, implying that the introduction of CuO onto the AC plays an important role on the enhancement of CO_2 adsorption. With increasing the CuO loading to 0.6 mmol/g AC, the CO_2 adsorption capacity of CuO/AC composites at 100 kPa increases to 2.11 mmol/g. With further increasing the CuO loading to 1.0 mmol/g AC, the CO_2 adsorption amount at 100 kPa decreases gradually to 1.73 mmol/g. This decrease is due to the excessive CuO species accumulation on the

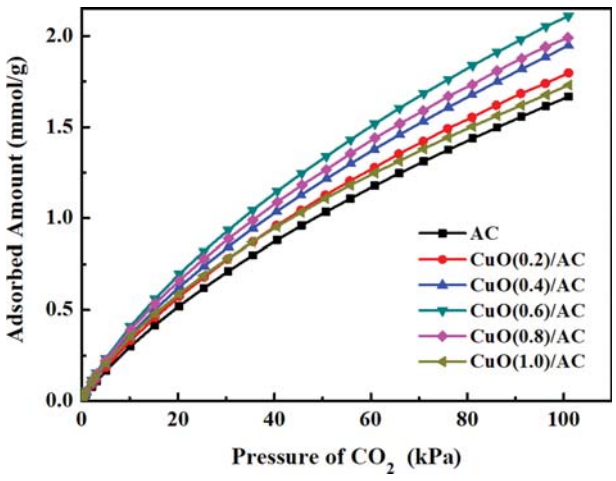

Fig. 4. Adsorption isotherms of CO_2 on AC support and CuO/AC composites with different CuO loadings at 303 K.

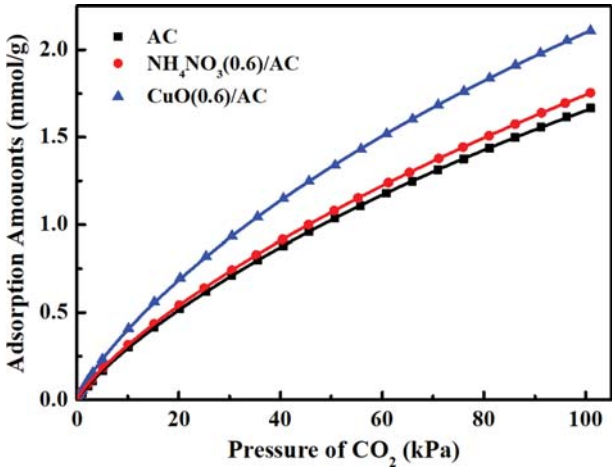

Fig. 5. Comparison of CO_2 adsorption capacity at 303 K of AC modified by NH_4NO_3 with that of AC support and AC modified by CuO.

surfaces of CuO(0.8)/AC and CuO(1.0)/AC composites, resulting in a pore channel blockage. In addition, during the activation process at high temperature, the decomposition of $Cu(NO_3)_2$ to CuO may release oxygen, and the released oxygen may react with AC, thus modifying the AC pore structure and affecting the CO_2 adsorption capacity. Thus, a comparative experiment of replacing $Cu(NO_3)_2$ with NH_4NO_3 in the same loading of 0.6 mmol/g AC was conducted to address this scenario, and the thermal decomposition of NH_4NO_3 only produces gaseous product and also releases oxygen. As shown in Fig. 5, after the modification by NH_4NO_3, the CO_2 adsorption capacity increases slightly compared to that of pure AC support, which may be due to the reaction of the released oxygen with AC, increasing the AC pore volumes. However, it can be seen that the CO_2 adsorption capacity of the adsorbent modified by NH_4NO_3 is much lower than that of the adsorbent modified by CuO, further highlighting the role of CuO in enhancing the CO_2 adsorption capacity.

In power plant flue gases, CO_2 and N_2 always exist together with a molar ratio of about 15 : 85. Therefore, an efficient adsorbent for the CO_2 separation from flue gases should achieve a high adsorption selectivity of CO_2/N_2. In this work, the CO_2 adsorption selectivity over N_2 on the CuO(0.6)/AC composite for the CO_2/N_2 mixture with a molar ratio of 15 : 85 was predicted by the IAST method from the adsorption data of pure CO_2 and N_2 and compared with the AC support. It can be seen from Fig. 6 that the prepared CuO/AC composite displays a high CO_2/N_2 adsorption selectivity, and as the adsorption pressure increases to 100 kPa the CO_2/N_2 adsorption selectivity decreases gradually from 79 to 58. In addition, in the entire measured pressure range, the CO_2/N_2 adsorption selectivity of CuO(0.6)/AC is markedly higher than that of the AC support, which indicates that the CuO species dispersed on the AC support plays a crucial role in the improvement of CO_2/N_2 adsorption selectivity. This phenomenon is ascribed to the fact that the π-complexation interactions between the CuO species dis-

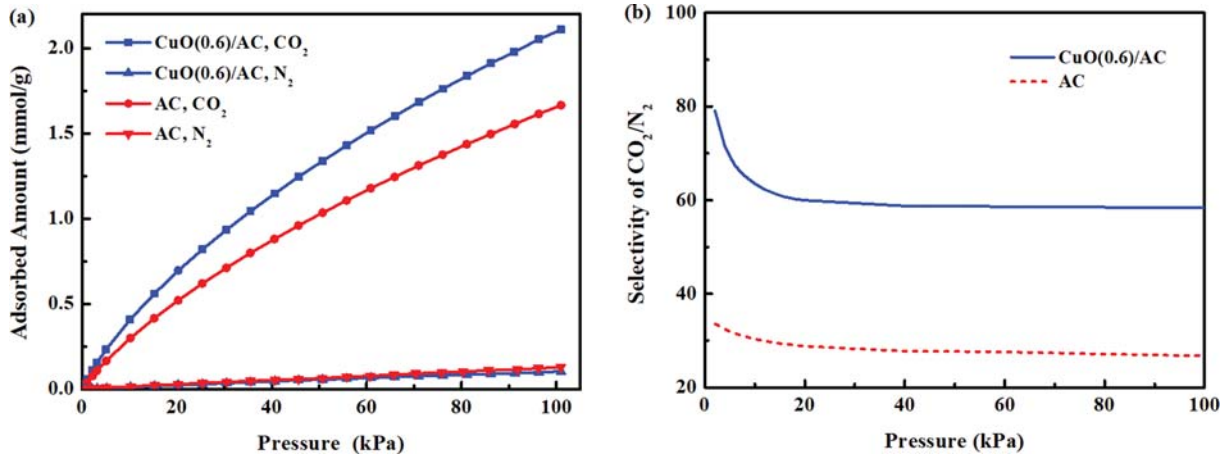

Fig. 6. Adsorption isotherms of CO_2 and N_2 on CuO(0.6)/AC and AC at 303 K (a) and CO_2/N_2 adsorption selectivity for the CO_2/N_2 (15 : 85) mixture (b).

Table 2. Comparison of CO_2 adsorption capacities at 100 kPa and 15 kPa, and CO_2/N_2 adsorption selectivity at 100 kPa on different adsorbents

Adsorbents	Adsorption capacity (mmol/g)		CO_2/N_2 selectivity	Refs.
	100 kPa	15 kPa		
Mg-MOF-74	8.55 (296 K)	6.20 (296 K)	182 (296 K)	49,50
UTSA-16	4.30 (296 K)	2.37 (296 K)	314 (296 K)	50
Cu-BTC	4.79 (298 K)	0.90 (298 K)	~50 (298 K)	51
Fe-MOF-74	2.41 (298 K)	0.57 (298 K)	~42 (298 K)	52
MIL-101(Cr)	2.33 (298 K)	0.57 (298 K)	~20 (298 K)	53
MIL-100(Fe)	2.25 (298 K)	0.60 (298 K)	6 (298 K)	54
Zeolite 13X	4.20 (298 K)	2.79 (298 K)	130 (298 K)	55
Beta	1.67 (303 K)	0.50 (303 K)	25.6 (303 K)	56
ZSM-5	1.33 (298 K)	0.50 (298 K)	~8 (298 K)	57
Zeolite Y	0.73 (303 K)	0.13 (303 K)	11 (303 K)	58
MCM-41	0.55 (298 K)	0.10 (298 K)	11 (298 K)	59
Norit R1 AC	2.24 (298 K)	0.44 (298 K)	8.8 (298 K)	60
BPL AC	1.91 (303 K)	0.46 (303 K)	~25 (298 K)	55,61
AC	1.64 (303 K)	0.40 (303 K)	25 (303 K)	This work
CuO(0.6)/AC	2.11 (303 K)	0.55 (303 K)	58 (303 K)	This work

persed on the CuO/AC composite and CO_2 molecules are stronger than the physisorption of the adsorbent with N_2. This higher adsorption selectivity makes the synthesized CuO/AC composite effectively separate CO_2 from the CO_2/N_2 mixture.

Table 2 gives a comparison of the CO_2 adsorption capacity and CO_2/N_2 adsorption selectivity on the prepared CuO@AC adsorbent in this work with some other reported adsorbents, such as MOFs and commercially available absorbents (e.g., activated carbons and zeolites). The CO_2 adsorption capacity at near 15 kPa is also an important parameter since the industrial flue gases usually contain ~15% CO_2, and this adsorption capacity is close to the CO_2 working capacity in a dynamic adsorption process for the CO_2/N_2 mixture with a molar ratio of 15 : 85 operating under atmospheric pressure [46]. Hence, the CO_2 adsorption capacity of the listed samples in Table 2 at 100 kPa and 15 kPa is summarized for comparison. Overall, the MOF materials, especially Mg-MOF-74, UTSA-16 and Cu-BTC, have higher CO_2 adsorption capacity and adsorption selectivity than other adsorbents. However, the industrial applications of the MOF material are very rare at present due to its expensive cost, poor durability and mechanical strength [47]. Compared with other zeolites and AC adsorbents in Table 2, the CuO(0.6)/AC adsorbent in this work exhibits a higher CO_2 adsorption capacity and CO_2/N_2 adsorption selectivity except zeolite 13X. However, the carbon material adsorbents present important advantages over zeolite 13X, such as hydrophobicity, significant lower cost, and lower energy requirements to carry out their regeneration. It was estimated that the capture cost per ton of CO_2 using zeolite 13X could reach US$51, while the capture cost using activated carbon is US$27 [48]. In addition, in this work, the preparation process of the CuO/AC adsorbent is facile and suitable for the industrial production. Nevertheless, at the low pressure of 15 kPa, the CO_2 adsorption capacity of the CuO(0.6)/AC adsorbent is still not ideal. This work mainly focuses on providing a facile method for the preparation of CuO/AC adsorbent and evaluating the effect of the introduction of CuO into AC support on the CO_2 adsorption performance. In our future work, the matrix and pore structure of the AC support will be optimized to further improve the CO_2 adsorption capacity of CuO/AC adsorbents at the low pressure.

In practical applications, the CO_2 adsorbents should possess a stable cyclic adsorption performance. Therefore, in order to verify the cyclic adsorption performance of the CuO(0.6)/AC composite, CO_2 adsorption at 303 K followed by the desorption under the vacuum at 473 K for 4 h on the composite was performed five times consecutively, and the result is presented in Fig. 7. After the five adsorption and desorption cycles, the CO_2 adsorption capacity of the CuO(0.6)/AC composite maintains the same adsorption capacity compared with the first cycle, demonstrating its excellent stability in the cyclic CO_2 adsorption. The above adsorption experimental results suggest that the synthesized CuO(0.6)/AC composite with the high CO_2 capture capability and adsorption selectivity, and the good cyclic adsorption capacity is a potential solid material for the CO_2 separation from flue gases.

In a practical TSA process for the CO_2 separation utilizing the obtained CuO(0.6)/AC adsorbent, the selection of a suitable reactor configuration is also crucial to effectively achieve a CO_2 multiple adsorption and desorption cycle. Generally, the adsorption separation process is carried out in several fixed-bed reactors, i.e., the adsorption operation on lean adsorbents is performed in part of the fixed-beds at the low temperature, and the regeneration operation on rich adsorbents is simultaneously performed in other fixed-beds at high temperature. For the proposed adsorbent in the powdered form in this work to be used in fixed bed operations, a previous pelletization step is needed to overcome the prohibitively high pressure drops. Thus, the powdered CuO/AC samples were shaped using poly (vinyl alcohol) as the binder with a 10% ratio, and the shaped samples were extruded into 2 mm strips and cut into 2-3 mm long column. However, it was found that the CO_2 adsorption capacity of the shaped adsorbent was reduced by about 15% compared with the unshaped adsorbent, attributed to the blockage of the partial pore channels by the binders, resulting in a decrease of the specific surface area and pore volume. In addition, the pelletization could lead to the additional intraparticle diffusion resistance, thus reducing the global adsorption kinetics. Gas-solid fluidized beds are the viable reactor configurations to process the fine powdered adsorbents, which are characterized by several advantages, such as high heat and mass transfer rates, good solids mixing, and ease in controlling and ensuring the uniformity of the bed temperature [62]. In particular, for the large heat releases and high demand on the heat management capability of the chemisorption process, a fluidized bed reactor is a suitable choice for ensuring nearly isothermal conditions. Pröll et al. [63] and Schöny et al. [64] proposed and evaluated a double loop multi-stage fluidized bed system for continuous CO_2 capture from flue gas streams by a TSA operation using solid adsorbents, and confirmed that the application of the double loop multi-stage system could significantly reduce the adsorbent circulation rate and the stripping gas demand compared to the single-stage fluidized bed systems, thus greatly reducing the energy demand of the CO_2 capture process. However, the fluidization of Geldart's group C ultrafine powders like the adsorbents prepared in this work using the conventional fluidization techniques is expected to be particularly difficult and qualitatively very poor, especially for high temperature applications, resulting from the strong interparticle cohesive forces (such as van der Waals,

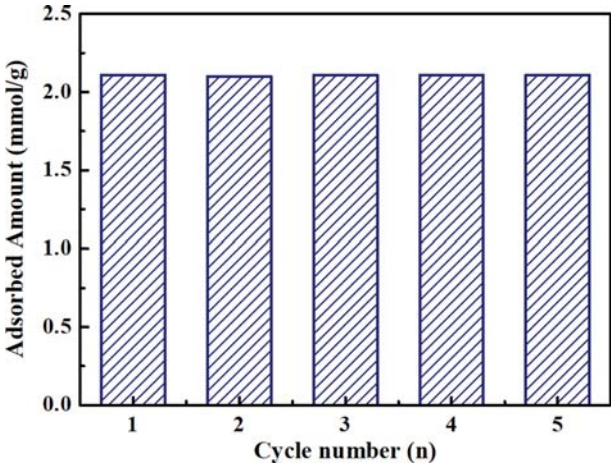

Fig. 7. The cyclic CO_2 adsorption capacity at 100 kPa on CuO(0.6)/AC with the adsorption at 303 K and desorption at 473 K.

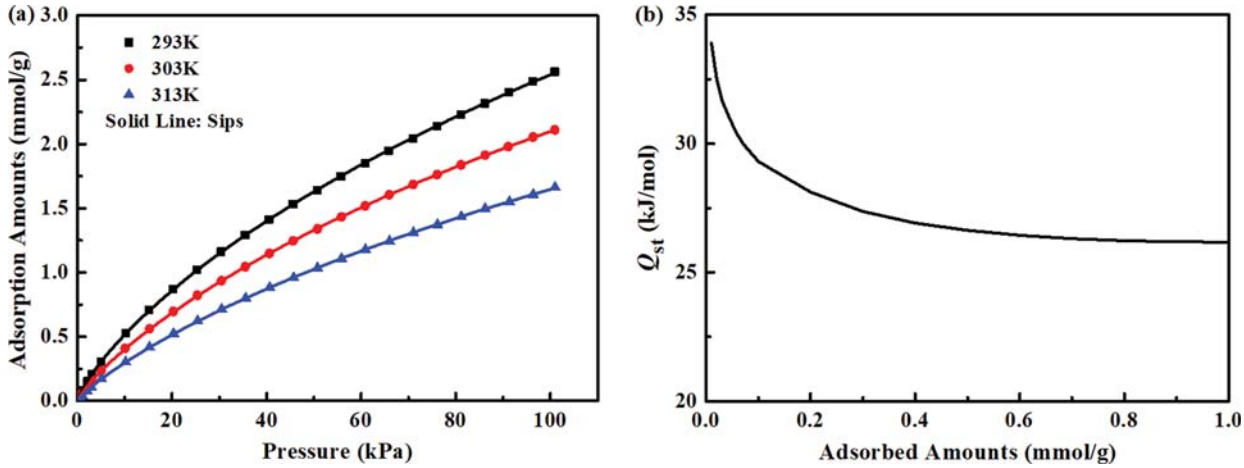

Fig. 8. CO_2 adsorption isotherms at different temperatures (a) and isosteric heats of adsorption for CO_2 on CuO(0.6)/AC as a function of CO_2 loading (b).

electrostatic and capillary forces), exhibiting the plug formation, channeling and agglomeration phenomena [65]. In this framework, the sound-assisted fluidization technique has been proved by Raganati et al. [66,67] to be a viable technological option to carry out TSA operations in the case of ultrafine powders. The application of proper acoustic fields can enhance the fine particles fluidization and gas-solid contact efficiency, and the sound wave can cause an efficient breakup of large aggregates yielded by interparticle cohesive forces, thus resulting in a disappearance of channeling and/or slugging, a uniform expansion of the bed and a improvement of fluidization quality [30,62]. Thus, the sound-assisted multi-stage fluidized bed system is a promising technological solution for the CO_2 capture utilizing the proposed adsorbent in this work.

To estimate the interaction of the CuO(0.6)/AC composite with CO_2 molecules, the adsorption isosteric heat was calculated from the experimental isotherm data at 293, 303 and 313 K (Fig. 8(a)) utilizing the Clausius-Clapeyron equation. The adsorption equilibrium data were correlated using the Sips equation, and the correlation coefficients are summarized in Table 3. From Fig. 8(a), the CO_2 adsorption capacity decreases with increasing the adsorption temperature, demonstrating an exothermic process of CO_2 adsorption on the CuO/AC composite. At a given CO_2 loading, the adsorption isosteric heat was calculated according to Eq. (3), and the calculated results at different CO_2 loadings are presented in Fig. 8(b). As shown in Fig. 8(b), the initial isosteric heat of adsorption is calculated to be 33.9 kJ/mol, which shows the strong interaction between the CuO(0.6)/AC composite and CO_2 molecules. With more CO_2 loading, the adsorption heat values decrease gradually over the entire loading range, indicative of the surface energetic heterogeneity of the used activated carbon support. In addition, the adsorption isosteric heat value is in the range of 27.3 to 33.9 kJ/mol, which is lower than that of chemical adsorption (60-90 kJ/mol) [68], suggesting that the regeneration of the CuO/AC composites will need a lower energy consumption. Hence, the CuO(0.6)/AC composite could realize a moderate operation temperature for the CO_2 separation from gas mixtures.

Table 3. Sips fitting parameters for CO_2 adsorption on CuO(0.6)/AC at different temperatures

Parameters	q_m (mmol/g)	$b \times 10^3$ (kPa^{-1})	n
CO_2 (293 K)	9.83	8.60	1.25
CO_2 (303 K)	8.67	7.42	1.22
CO_2 (313 K)	7.14	6.30	1.19

CONCLUSIONS

A series of CuO/AC composites with various CuO contents for the CO_2 capture have been successfully synthesized using $Cu(NO_3)_2$ as the copper source by a facile solid-state heat dispersion method. The XRD and SEM results indicate that after the activation at high temperatures, the $Cu(NO_3)_2$ precursor was well dispersed into the AC pore channels and converted into the highly dispersed CuO. After the introduction of CuO, the synthesized CuO(0.6)/AC composite achieves an enhancement in CO_2 adsorption capacity and CO_2/N_2 adsorption selectivity compared with the AC support, which are 2.11 mmol/g and 58 at 303 K and 100 kPa, respectively. Moreover, this composite displays a good stability in CO_2 adsorption cycles and could realize a moderate operation temperature. The facile synthesis process and good CO_2 adsorption performance make the synthesized CuO(0.6)/AC composite a potential solid adsorbent for the CO_2 separation.

CONFLICT OF INTEREST STATEMENT

There are no conflicts to declare.

ACKNOWLEDGEMENTS

This work was supported by the Qingdao Science and Technology Plan Application Foundation Research Project (19-6-2-28-cg), the Natural Science Foundation of Shandong Province (ZR2018BB071) and the Shandong Provincial Key Research and Development Program (2019GSF109038).

REFERENCES

1. X. S. Zheng, D. Streimikiene, T. Balezentis, A. Mardani, F. Cavallaro and H. Liao, *J. Clean. Prod.*, **234**, 1113 (2019).
2. Z. Wang, N. Goyal, L. Liu, D. C. W. Tsang, J. Shang, W. Liu and G. Li, *Chem. Eng. J.*, **396**, 125376 (2020).
3. N. Li, X. Zhang, M. Shi and S. Zhou, *Resour. Conserv. Recy.*, **121**, 11 (2017).
4. M. Zaman and J. H. Lee, *Korean J. Chem. Eng.*, **30**, 1497 (2013).
5. J. L. Míguez, J. Porteiro, R. Pérez-Orozco, D. Patiño and S. Rodríguez, *Appl. Energy*, **211**, 1282 (2018).
6. B. Liu, M. Zhang, X. Yang and T. Wang, *J. Taiwan Inst. Chem. E.*, **103**, 67 (2019).
7. C. Manianglung, R. M. Pacia and Y. S. Ko, *Korean J. Chem. Eng.*, **36**, 1267 (2019).
8. A. B. Rao and E. S. Rubin, *Environ. Sci. Technol.*, **36**, 4467 (2002).
9. J. D. Figueroa, T. Fout, S. Plasynski and H. McIlvried, *Int. J. Greenh. Gas Con.*, **2**, 9 (2008).
10. S. Bae, N. Zaini, K. S. N. Kamarudin, K. S. Yoo, J. Kim and M. R. Othman, *Korean J. Chem. Eng.*, **35**, 764 (2018).
11. Q. Wang, J. Z. Luo, Z. Y. Zhou and A. Borgna, *Energy Environ. Sci.*, **4**, 42 (2011).
12. Y. Wang, T. Du, X. Fang, D. Meng, G. Li and L. Liu, *Korean J. Chem. Eng.*, **35**, 1642 (2018).
13. F. Montagnaro, A. Silvestre-Albero, J. Silvestre-Albero, F. Rodríguez-Reinoso, A. Erto, A. Lancia and M. Balsamo, *Micropor. Mesopor. Mater.*, **209**, 157 (2015).
14. S. Wang, Y. Xu, J. Miao, M. Liu, B. Ren, L. Zhang and Z. Liu, *J. Clean. Prod.*, **253**, 120023 (2020).
15. C. S. Lee, Y. L. Ong, M. K. Aroua and W. M. A. W. Daud, *Chem. Eng. J.*, **219**, 558 (2013).
16. H. Burri, R. Anjum, R. B. Gurram, H. Mitta, S. Mutyala and M. Jonnalagadda, *Korean J. Chem. Eng.*, **36**, 1482 (2019).
17. J. Sreńscek-Nazzal and K. Kiełbasa, *Appl. Surf. Sci.*, **494**, 137 (2019).
18. X. E. Hu, L. Liu, X. Luo, G. Xiao, E. Shiko, R. Zhang, X. Fan, Y. Zhou, Y. Liu, Z. Zeng and C. Li, *Appl. Energy*, **260**, 114244 (2020).
19. S. Mutyala, S. M. Yakout, S. S. Ibrahim, M. Jonnalagadda and H. Mitta, *New J. Chem.*, **43**, 9725 (2019).
20. J. Zhang, R. Singh and P. A. Webley, *Micropor. Mesopor. Mater.*, **111**, 478 (2008).
21. K. Upendar, A. Sri Hari Kumar, N. Lingaiah, K. S. Rama Rao and P. S. Sai Prasad, *Int. J. Greenh. Gas Con.*, **10**, 191 (2012).
22. J. Ding, C. Yu, J. Lu, X. Wei, W. Wang and G. Pan, *Appl. Energy*, **263**, 114681 (2020).
23. B. Zhao, L. Ma, H. Shi, K. Liu and J. Zhang, *J. CO_2 Util.*, **25**, 315 (2018).
24. K. C. Chanapattharapol, S. Krachuamram and S. Youngme, *Micropor. Mesopor. Mater.*, **245**, 8 (2017).
25. D. I. Jang and S. J. Park, *Fuel*, **102**, 439 (2012).
26. B.-J. Kim, K.-S. Cho and S.-J. Park, *J. Colloid Interface Sci.*, **342**, 575 (2010).
27. M. Li, K. Huang, J. A. Schott, Z. Wu and S. Dai, *Micropor. Mesopor. Mater.*, **249**, 34 (2017).
28. M. Sun, Q. Gu, A. Hanif, T. Wang and J. Shang, *Chem. Eng. J.*, **370**, 1450 (2019).
29. N. Tlili, G. Grévillot and C. Vallières, *Int. J. Greenh. Gas Control*, **3**, 519 (2009).
30. F. Raganati, R. Chirone and P. Ammendola, *Ind. Eng. Chem. Res.*, **59**, 3593 (2020).
31. F. Raganati, M. Alfe, V. Gargiulo, R. Chirone and P. Ammendola, *Chem. Eng. J.*, **372**, 529 (2019).
32. J. Bonjour, J.-B. Chalfen and F. Meunier, *Ind. Eng. Chem. Res.*, **41**, 5802 (2002).
33. R. T. Yang, *Adsorbents: Fundamentals and applications*, John Wiley & Sons, Hoboken (2003).
34. P.-T. Huong and B.-K. Lee, *Micropor. Mesopor. Mater.*, **241**, 155 (2017).
35. A. Somy, M. R. Mehrnia, H. D. Amrei, A. Ghanizadeh and M. Safari, *Int. J. Greenh. Gas Con.*, **3**, 249 (2009).
36. K. Cho, J. Kim, H. T. Beum, T. Jung and S. S. Han, *J. Hazard. Mater.*, **344**, 857 (2018).
37. F. Gao, Y. Wang, X. Wang and S. Wang, *Adsorption*, **22**, 1013 (2016).
38. H. M. F. Freundlich, *J. Phys. Chem.*, **57**, 385 (1906).
39. I. Langmuir, *J. Am. Chem. Soc.*, **40**, 1361 (1918).
40. R. Sips, *J. Chem. Phys.*, **16**, 490 (1948).
41. J. Toth, *Acta Chem. Acad. Hung.*, **69**, 311 (1971).
42. A. L. Myers and J. M. Prausnitz, *AIChE J.*, **11**, 121 (1965).
43. P. Su, X. Zhang, Z. Xu, G. Zhang, C. Shen and Q. Meng, *New J. Chem.*, **43**, 17267 (2019).
44. K. Pirzadeh, K. Esfandiari, A. A. Ghoreyshi and M. Rahimnejad, *Korean J. Chem. Eng.*, **37**, 513 (2020).
45. J. Yin, J. Cai, C. Yin, L. Gao and J. Zhou, *J. Environ. Chem. Eng.*, **4**, 958 (2016).
46. Y. Chen, H. Wu, D. Lv, W. Yang, Z. Qiao, Z. Li and Q. Xia, *Energy Fuels*, **32**, 8676 (2018).
47. S. Y. Lee and S. J. Park, *J. Ind. Eng. Chem.*, **23**, 1 (2015).
48. M. G. Plaza, S. García, F. Rubiera, J. J. Pis and C. Pevida, *Chem. Eng. J.*, **163**, 41 (2010).
49. J. A. Mason, K. Sumida, Z. R. Herm, R. Krishna and J. R. Long, *Energy Environ. Sci.*, **4**, 3030 (2011).
50. S. Xiang, Y. He, Z. Zhang, H. Wu, W. Zhou, R. Krishna and B. Chen, *Nat. Commun.*, **3**, 954 (2012).
51. Y. Wu, Z. Lv, X. Zhou, J. Peng, Y. Tang and Z. Li, *Chem. Eng. J.*, **355**, 815 (2019).
52. W. Lou, J. Yang, L. Li and J. Li, *J. Solid State Chem.*, **213**, 224 (2014).
53. Z. Zhou, L. Mei, C. Ma, F. Xu, J. Xiao, Q. Xia and Z. Li, *Chem. Eng. J.*, **147**, 109 (2016).
54. L. Mei, T. Jiang, X. Zhou, Y. Li, H. Wang and Z. Li, *Chem. Eng. J.*, **321**, 600 (2017).
55. J. McEwen, J.-D. Hayman and A. Ozgur Yazaydin, *Chem. Phys.*, **412**, 72 (2013).
56. X. Xu, X. Zhao, L. Sun and X. Liu, *J. Nat. Gas Chem.*, **17**, 391 (2008).
57. M. Hefti, D. Marx, L. Joss and M. Mazzotti, *Micropor. Mesopor. Mater.*, **215**, 215 (2015).
58. F. Gao, S. Wang, G. Chen, J. Duan, J. Dong and W. Wang, *Adsorption*, **26**, 701 (2020).
59. Y. Belmabkhout and A. Sayari, *Chem. Eng. Sci.*, **64**, 3729 (2009).
60. S. Beutekamp and P. Harting, *Adsorption*, **8**, 255 (2002).
61. P. Brea, J. A. Delgado, V. I. Águeda and M. A. Uguina, *Chem. Eng. J.*, **355**, 279 (2019).
62. F. Raganati, R. Chirone and P. Ammendola, *Chem. Eng. Res. Des.*, **133**, 347 (2018).

63. T. Pröll, G. Schöny, G. Sprachmann and H. Hofbauer, *Chem. Eng. Sci.*, **141**, 166 (2016).
64. G. Schöny, F. Dietrich, J. Fuchs, T. Pröll and H. Hofbauer, *Powder Technol.*, **316**, 519 (2017).
65. F. Raganati, R. Chirone and P. Ammendola, *Ind. Eng. Chem. Res.*, **56**, 12811 (2017).
66. P. Ammendola, F. Raganati and R. Chirone, *Fuel Process. Technol.*, **134**, 494 (2015).
67. F. Raganati, P. Ammendola and R. Chirone, *Sep. Purif. Technol.*, **167**, 24 (2016).
68. W. Liang, Z. Liu, J. Peng, X. Zhou, X. Wang and Z. Li, *Energy Fuels*, **33**, 493 (2019).